

Inclusive electron scattering off ^{12}C , ^{40}Ca , and ^{40}Ar : effects of the meson exchange currents

A. V. Butkevich and S. V. Luchuk

Institute for Nuclear Research,

Russian Academy of Sciences,

Moscow 117312, Russia

(Dated: September 22, 2020)

The scattering of electrons on carbon, calcium, and argon targets are analyzed using an approach that incorporates the contributions to the electromagnetic response functions from the quasielastic (QE), inelastic processes, and two-particle and two-hole meson exchange current (2p-2h MEC). This approach describes well the whole energy spectrum of data at very different kinematics. It is shown that the accuracy of the (e, e') cross section calculations in the region between the QE and delta-resonance peaks, where the 2p-2h MEC contribution reaches its maximum value, depends on the momentum transfer $|\mathbf{q}|$ and at $|\mathbf{q}| > 500$ MeV the calculated and measured cross sections are in agreement within the experimental uncertainties.

PACS numbers: 25.30.-c, 25.30.Bf, 25.30.Pt, 13.15.+g

I. INTRODUCTION

The current [1, 2] and future [3, 4] long-baseline neutrino experiments aim at measuring the lepton CP violation phase, improving the accuracy of the value of the mixing angle θ_{23} , and determining neutrino mass ordering. To evaluate the oscillation parameters, the probabilities of neutrino oscillations as functions of neutrino energy are measured. The neutrino beams are not monoenergetic and have broad distributions that range from tens of MeVs to a few GeVs. This is one of the problems in achieving a high level of accuracy of the oscillation parameters measurements.

In this energy range, charged-current (CC) quasielastic (QE) scattering induced by both one- and two-body currents and resonance production are the main contributions to the

neutrino-nucleus scattering. The incident neutrino energy is reconstructed using calorimetric methods, which rely not only on the visible energy measured in the detector, but also on the models of the neutrino-nucleus interactions that are implemented in neutrino event generators. In addition to its role in the reconstruction of the neutrino energy, the neutrino-nucleus scattering model is critical for obtain background estimates, and for correct extrapolations of the near detector constraints to the far detector in analyses aimed at determining the neutrino oscillation parameters.

The modeling of neutrino-nucleus interactions in the energy range $\varepsilon_\nu \approx 0.2\text{--}5$ GeV is one of the most complicated issues facing neutrino oscillation experiments. The description of nuclear effects is one of the largest sources of systematic uncertainties despite use of the near detector for tuning the nuclear models employed in the neutrino events generator. A significant systematic uncertainty arises from the description of scattering induced by the two body meson exchange currents (MEC), which may produce two-particle and two-hole final states. Such excitations are induced by two-body currents, hence, they go beyond the impulse approximation scheme in which the probe interacts with only a single nucleon and corresponds to the 1p-1h excitations. A poor modelling of these MEC processes leads to a bias in the reconstruction of neutrino energy and thereby to large systematic uncertainties in the neutrino oscillation parameters [5].

In recent years many studies have been presented to improve our knowledge on lepton-nucleus scattering [6–10, 12–28]. Approaches which go beyond the impulse approximation were developed in Refs. [11–15, 19, 20, 22, 23, 26]. As neutrino beams have broad energy distributions, various contributions to the cross sections can significantly overlap with each other making it difficult to identify, diagnose and remedy shortcoming of nuclear models. On the other hand, in electron-scattering the energy and momentum transfer are known and therefore measurements in kinematic ranges and on targets of interest to neutrino experiments give an opportunity to validate and improve the description of nuclear effects. Electron beams can be used to investigate physics corresponding to different interaction mechanisms, by measuring the nuclear response at energy transfers varied independently from three-momentum transfer. The neutrino detectors are typically composed of scintillator, water, or argon. There is a large body of electron-scattering data on carbon and calcium and only a few data sets available for scattering on argon.

Weak interactions of neutrino probe the nucleus in a similar way as electromagnetic elec-

tron interactions. The vector part of the electroweak interaction can be inferred directly from electron-scattering and the influence of nuclear medium is the same as in neutrino-nucleus scattering. Precise electron-scattering data give unique opportunity to validate nuclear model employed in neutrino physics. A model unable to reproduce electron measurements cannot be expected to provide accurate predictions for neutrino cross sections. So, the detailed comparison with electron scattering data (semi-inclusive and inclusive cross sections and response functions) is a necessary test for any theoretical models used to describe of the lepton-nucleus interaction.

In this work we test a joint calculation of the QE, 2p-2h MEC, and inelastic scattering contributions (RDWIA+MEC+RES approach) on carbon, calcium, and argon, using the relativistic distorted-wave impulse approximation (RDWIA) [29–31] for quasi-elastic response and meson exchange currents response functions for 2p-2h final states presented in Ref.[16]. For calculation of inelastic contributions to the cross sections we adopt parameterizations for the single-nucleon inelastic structure functions given in Refs.[32, 33], which provide a good description of the resonant structure in (e, e') cross sections and cover a wide kinematic region. We compare the RDWIA+MEC+RES predictions with the whole energy spectrum of (e, e') data, including the recent JLab data for electron scattering on carbon and argon. We also perform a comparison and analysis of the calculated cross sections and data at the momentum transfer that corresponds to the region between the QE and Δ -resonance peak, where the 2p-2h response is peaked.

In Sec.II we briefly introduce the formalism needed for studying electron scattering off nuclei with quasielastic, 2p-2h MEC, and resonance production contributions. We also describe briefly the basic aspects of the models used for the calculations. The results are presented and discussed in Sec.III. Our conclusions are summarized in Sec.IV.

II. FORMALISM OF ELECTRON-NUCLEUS SCATTERING, RDWIA, 2p-2h MEC, AND INELASTIC RESPONSES

We consider the inclusive electron-nucleus scattering

$$e(k_i) + A(p_A) \rightarrow e'(k_f) + X \quad (1)$$

in the one-photon exchange approximation. Here $k_i = (\varepsilon_i, \mathbf{k}_i)$ and $k_f = (\varepsilon_f, \mathbf{k}_f)$ are the initial and final lepton momenta, $p_A = (\varepsilon_A, \mathbf{p}_A)$ is the initial target momentum, $q = (\omega, \mathbf{q})$ is the momentum transfer carried by the virtual photon, and $Q^2 = -q^2 = \mathbf{q}^2 - \omega^2$ is the photon virtuality.

A. Electron-nucleus cross sections

In the inclusive reactions (1) only the outgoing lepton is detected and the differential cross section can be written as

$$\frac{d^3\sigma}{d\varepsilon_f d\Omega_f} = \frac{\varepsilon_f}{\varepsilon_i} \frac{\alpha^2}{Q^4} L_{\mu\nu} W^{\mu\nu}, \quad (2)$$

where $\Omega_f = (\theta, \phi)$ is the solid angle for the electron momentum, $\alpha \approx 1/137$ is the fine-structure constant, $L_{\mu\nu}$ is the lepton tensor, and $W^{\mu\nu}$ is the electromagnetic nuclear tensor. In terms of the longitudinal R_L and transverse R_T nuclear response functions the cross section reduces to

$$\frac{d^3\sigma}{d\varepsilon_f d\Omega_f} = \sigma_M (V_L R_L + V_T R_T), \quad (3)$$

where

$$\sigma_M = \frac{\alpha^2 \cos^2 \theta / 2}{4\varepsilon_i^2 \sin^4 \theta / 2} \quad (4)$$

is the Mott cross section. The coupling coefficients

$$V_L = \frac{Q^4}{\mathbf{q}^4}, \quad (5a)$$

$$V_T = \left(\frac{Q^2}{2\mathbf{q}^2} + \tan^2 \frac{\theta}{2} \right), \quad (5b)$$

are kinematic factors depending on the lepton's kinematics. The response functions are given in terms of components of the hadronic tensors

$$R_L = W^{00}, \quad (6a)$$

$$R_T = W^{xx} + W^{yy}, \quad (6b)$$

and depend on the variables (Q^2, ω) or $(|\mathbf{q}|, \omega)$. They describe the electromagnetic properties of the hadronic system. The relations between the response functions and cross sections for longitudinally σ_L and transversely σ_T polarized virtual photons are

$$R_L = \frac{K}{(2\pi)^2 \alpha} \left(\frac{\mathbf{q}^2}{Q^2} \right) \sigma_L, \quad (7a)$$

$$R_T = \frac{K}{2\pi^2\alpha}\sigma_T, \quad (7b)$$

where $K = \omega - Q^2/2m$ is the equivalent energy of a real photon needed to produce the same final mass state and m is the mass of nucleon.

All the nuclear structure information and final state interaction effects (FSI) are contained in the electromagnetic nuclear tensor. It is given by expression

$$W_{\mu\nu} = \sum_f \langle X | J_\mu | A \rangle \langle A | J_\nu^\dagger | X \rangle, \quad (8)$$

where J_μ is the nuclear electromagnetic current operator that connects the initial nucleus state $|A\rangle$ and the final state $|X\rangle$. The sum is taken over the scattering states corresponding to all of allowed asymptotic configurations. This equation is very general and includes all possible channels. Thus, the hadron tensor can be expanded as the sum of the 1p-1h and 2p-2h, plus additional channels, including the inelastic electron-nucleus scattering W_{in} :

$$W^{\mu\nu} = W_{1p1h}^{\mu\nu} + W_{2p2h}^{\mu\nu} + W_{in}^{\mu\nu} \dots \quad (9)$$

The hadronic tensors W_{1p1h} , W_{2p2h} , and W_{in} determine, correspondingly, the QE, 2p-2h MEC, and inelastic response functions. Therefore, the functions R_i in Eq.(6) can be written as a sum of the QE ($R_{i,QE}$), MEC ($R_{i,MEC}$), and inelastic response functions ($R_{i,in}$)

$$R_i = R_{i,QE} + R_{i,MEC} + R_{i,in} \quad (10)$$

B. Model

We describe genuine QE electron-nuclear scattering within the RDWIA approach. This formalism is entirely based on the impulse approximation, namely one body currents. In this approximation the nuclear current is written as a sum of single-nucleon currents and nuclear matrix element in Eq. (8) takes the form

$$\langle p, B | J^\mu | A \rangle = \int d^3r \exp(i\mathbf{t} \cdot \mathbf{r}) \bar{\Psi}^{(-)}(\mathbf{p}, \mathbf{r}) \Gamma^\mu \Phi(\mathbf{r}), \quad (11)$$

where Γ^μ is the vertex function, $\mathbf{t} = \varepsilon_B \mathbf{q}/W$ is the recoil-corrected momentum transfer, $W = \sqrt{(m_A + \omega)^2 - \mathbf{q}^2}$ is the invariant mass and Φ and $\Psi^{(-)}$ are relativistic bound-state and outgoing wave functions.

For electron scattering, we use the electromagnetic vertex function for a free nucleon

$$\Gamma^\mu = F_V(Q^2)\gamma^\mu + i\sigma^{\mu\nu}\frac{q_\nu}{2m}F_M(Q^2), \quad (12)$$

where $\sigma^{\mu\nu} = i[\gamma^\mu, \gamma^\nu]/2$, F_V and F_M are the Dirac and Pauli nucleon form factors. We use the approximation of Ref. [34] for the Dirac and Pauli nucleon form factors and employ the de Forest prescription [35] and Coulomb gauge for the off-shell vector current vertex Γ^μ , because the bound nucleons are off-shell.

In RDWIA calculations the independent particle shell model (IPSM) is assumed for the nuclear structure. In Eq.(11) the relativistic bound-state wave function for nucleons Φ are obtained as the self-consistent solutions of a Dirac equation, derived within a relativistic mean-field approach, from a Lagrangian containing σ , ω , and ρ mesons [36]. The nucleon bound-state functions were calculated by the TIMORA code [37] with the normalization factors S relative to full occupancy of the IPSM orbitals. For carbon an average factor $\langle S \rangle \approx 89\%$ is used, and for ^{40}Ca and ^{40}Ar the occupancy is $\langle S \rangle \approx 87\%$ on average. These estimations of the depletion of the hole state follows from the RDWIA analysis of $^{12}\text{C}(e, e'p)$ [38, 39] and $^{40}\text{Ca}(e, e'p)$ [16]. In this work we assume that the source of the reduction of the $(e, e'p)$ spectroscopic factors with respect to the mean field values are the NN short-range and tensor correlations in the ground state, leading to the appearance of the high-momentum and high-energy component in the nucleon distribution in the target.

In the RDWIA, final state interaction effects for the outgoing nucleon are taken into account. The distorted-wave function of the knocked out nucleon Ψ is evaluated as a solution of a Dirac equation containing a phenomenological relativistic optical potential. This potential consists of a real part, which describes the rescattering of the ejected nucleon and an imaginary part for the absorption of it into unobserved channels. The EDAD1 parameterization [40] of the relativistic optical potential for carbon and calcium was used in this work. A complex optical potential with a nonzero imaginary part generally produces an absorption of the flux. However, for the inclusive cross section, the total flux must be conserved. The inclusive responses (i.e., no flux lost) can be handled by simply removing the imaginary terms in the potential. This yields results that are almost identical to those calculate via relativistic Green's function approach [41, 42] and Green's function Monte Carlo method [43] in which the FSI effects are treated by means of complex potential and total flux is conserved.

The inclusive cross sections with the FSI effects, taking into account the NN correlations were calculated using the method proposed in Ref. [8] with the nucleon high-momentum and high-energy distribution from Ref. [44] renormalized to value of 11% for carbon and of 13% for calcium and argon. The contribution of the NN -correlated pairs is evaluated in the impulse approximation, i.e., the virtual photon couples to only one member of the NN pair. It is a one-body current process that leads to the emission of two nucleons (2p-2h excitation).

The evaluation of the 2p-2h MEC contributions is performed within the relativistic Fermi gas model [18, 45]. The short-range NN -correlations and FSI effects were not considered in this approach. The elementary hadronic tensor $W_{2p2h}^{\mu\nu}$ is given by the bilinear product of the matrix elements of the two-body electromagnetic MEC. Only one-pion exchange is included. The two-body current operator is obtained from the electroweak pion production amplitudes for the nucleon [46] with the coupling a second nucleon to the emitted pion. The two-body electromagnetic current is the sum of seagull, pion-in-flight, and Delta-pole currents. The seagull terms are associated with the interaction of the virtual photon at the $NN\pi$ vertex, whereas the pion-in-flight operator is referred to the direct interaction of photon with the virtual pion. The Δ peak is the main contribution to the pion production cross section. However, inside the nucleus Δ can also decay into one nucleon that rescatters producing two-nucleon emission without pions. As a result, the MEC peak is located in the dip region between the QE and Delta peaks, i.e., the invariant mass of the pion-nucleon pair $W^2 = (q + p_A)^2 = m^2 + 2m\omega - Q^2$ varies in the range $(m_\pi + m) \leq W \leq 1.3 - 1.4$ GeV, where m_π is the mass of pion.

The exact evaluation of the 2p-2h hadronic tensor in a fully relativistic way performed in Refs. [18, 45] is highly non-trivial. In the present work we evaluate the electromagnetic MEC response functions $R_{i,MEC}$ of electron scattering on carbon using accurate parameterizations of the exact MEC calculations. The 2p-2h MEC contributions for ^{40}Ca and ^{40}Ar were calculated using the parameterization for ^{12}C rescaled for calcium and argon according to Ref. [47]. The parameterization form employed for the different electroweak responses is the function of $(\omega, |\mathbf{q}|)$ and valid in the range of momentum transfer $|\mathbf{q}| = 200\text{--}2000$ MeV. The expressions for the fitting parameters are described in detail in Refs. [20, 21, 48].

Finally, the inelastic response functions $R_{i,in}$ were calculated using the parameterization for the neutron [32] and proton [33] structure functions. This approach is based on an

empirical fit to describe the measurements of inelastic electron-proton and electron-deuteron cross sections in the kinematic range of four-momentum transfer $0 < Q^2 < 8 \text{ GeV}^2$ and final state invariant mass $1.1 < W_x < 3.1 \text{ GeV}$, thus starting from pion production region to the highly-inelastic region. These fits are constrained by the high precision longitudinal σ_L and transverse σ_T separated cross section measurements and provide a good description of the structures seen in inclusive (e, e') cross sections.

III. RESULTS AND ANALYSIS

Before providing reliable predictions for neutrino scattering, any model must be validated by confronting it with electron scattering data. The agreement between the model's predictions and data in the vector sector of electroweak interaction gives us confidence in the extension of this phenomenological approach and its validity at least in the vector sector of the electroweak interaction.

To test the RDWIA+MEC+RES approach we calculated the double-differential inclusive $^{12}\text{C}(e, e')$, $^{40}\text{Ca}(e, e')$, and $^{40}\text{Ar}(e, e')$ cross sections as functions of the energy transfer to the nucleus. Results for carbon and calcium are shown in Figs. 1 and 2, respectively, and compared with data from Refs. [49–56]. Each panel corresponds to the fixed values of the incident electron energy E and scattering angle θ . The kinematical coverage includes both quasielastic peak, dip region, and extends to the region of the delta-production peak.

In Figs. 1 and 2 we show the separate contributions to the inclusive cross section from QE (dot-dashed line), 2p-2h MEC (dashed line), and inelastic (dotted line) processes. The total contribution is presented by a solid line. The panels have been ordered according to the corresponding value for the momentum transfer at the quasielastic peak q_{QE} . This corresponds to the value of $|\mathbf{q}|$ where the maximum in the QE peak appears. The q_{QE} runs from $\approx 310 \text{ MeV}$ to $\approx 590 \text{ MeV}$ for carbon and $340 < q_{QE} < 600 \text{ MeV}$ for calcium.

The systematic analysis presented in Figs. 1 and 2 shows that the RDWIA+MEC+RES approach leads to a good description of the whole set of (e, e') data, validating the reliability of our predictions. The positions, widths, and heights of the QE peak are reproduced by the model within the experimental errors, taking into account not only the QE domain but also the contributions given by the 2p-2h MEC and inelastic terms. Notice that the dip region is also successfully reproduced by the theory. Only at the lower value of $q_{QE} < 340 \text{ MeV}$ the

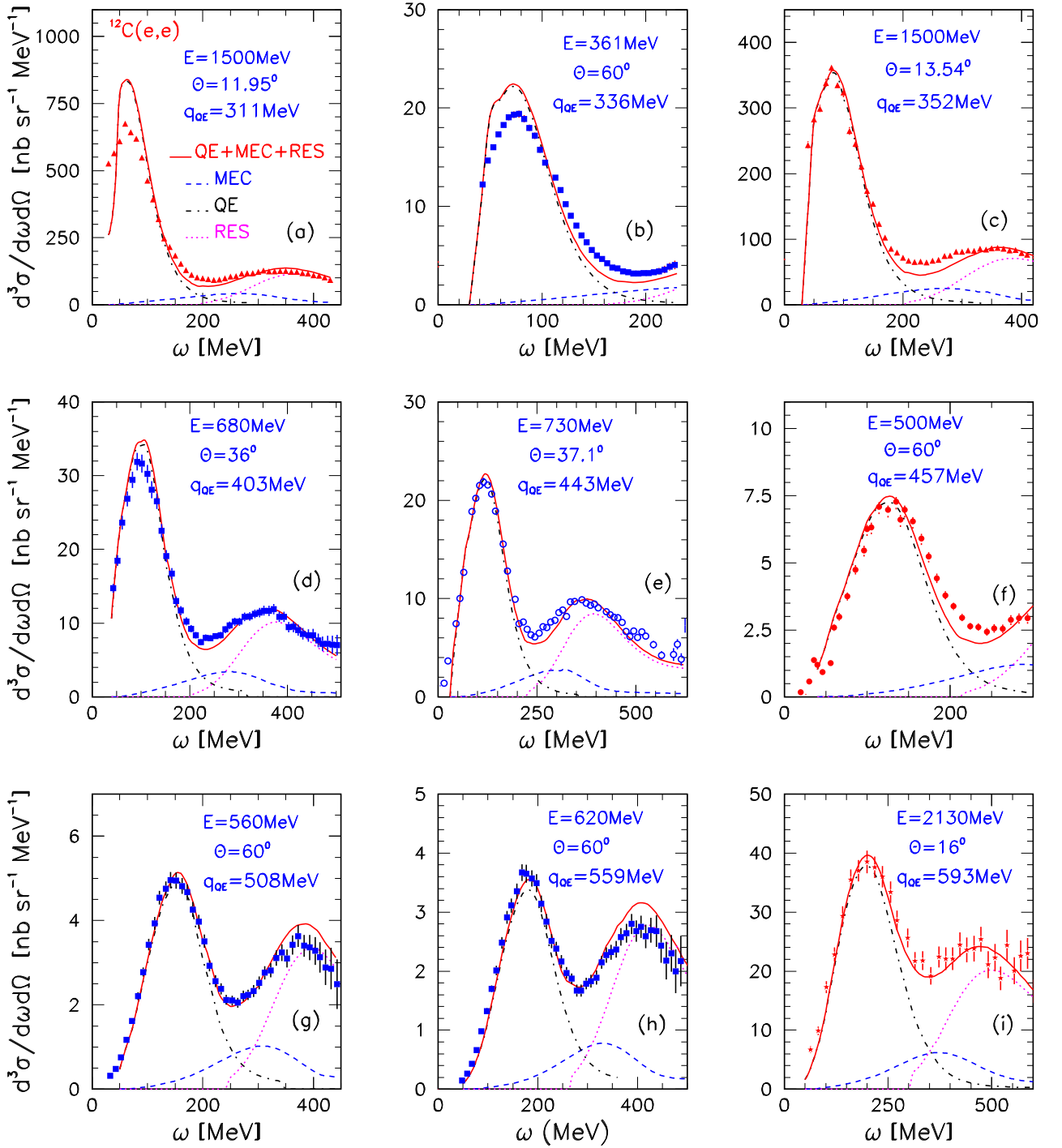


FIG. 1: The $^{12}\text{C}(e, e')$ double differential cross sections as functions of energy transfer ω compared with the RDWIA+MEC+RES predictions. The data are from Ref. [52] (filled triangles), Ref. [49] (filled squares), Ref. [51] (open circles), Ref. [50] (filled circles), Ref. [54, 55] (stars).

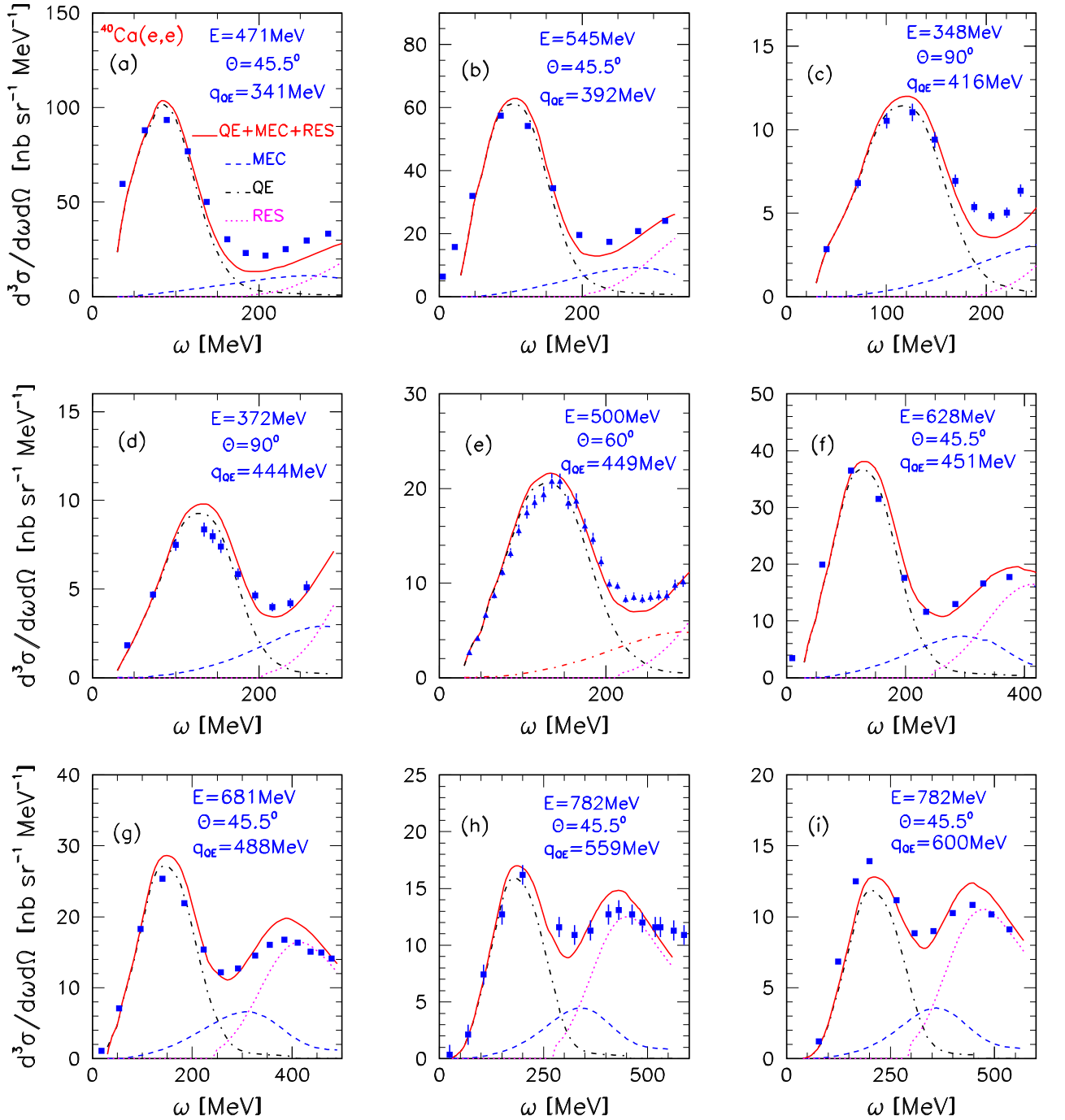


FIG. 2: The $^{12}\text{Ca}(e,e')$ double differential cross sections as functions of energy transfer ω compared with the RDWIA+MEC+RES predictions. The data are from Ref. [56] (filled squares) and Ref. [50] (filled triangles).

theoretical predictions for carbon overestimate data by 30-50% at the QE peak, and this should be expected since this is the region where the impulse approximation conditions may not be satisfied and collective nuclear effects are important.

The agreement between theory and data in the inelastic region also is good within the experimental uncertainties. The inelastic part of the cross section is dominated by the Δ peak that contributes to the transverse response function. In particular, $\omega_{QE} = \sqrt{|\mathbf{q}|^2 + m^2} - m$ corresponds roughly to the center of the quasielastic peak, and $\omega_{\Delta} = \sqrt{|\mathbf{q}|^2 + m_{\Delta}^2} - m$ to the Δ -resonance [m_{Δ} is the mass of $\Delta(1232)$]. When the momentum transfer is not too high these regions are clearly separated in data

$$\Delta\omega = \omega_{\Delta} - \omega_{QE} = \frac{(m_{\Delta}^2 - m^2)}{\sqrt{|\mathbf{q}|^2 + m^2} + \sqrt{|\mathbf{q}|^2 + m_{\Delta}^2}}, \quad (13)$$

allowing for a test of theoretical models for each specific process. On the other hand, for increasing values of the momentum transfer the peaks corresponding to the Δ and QE domains become closer, and their overlap increases significantly. In this case only the comparison with a complete model including inelastic processes is meaningful.

In addition to the previous analysis, we have also tested the validity of the RD-WIA+MEC+RES approach through the analysis of the recent JLab data [57, 58] for inclusive electron scattering data on carbon and argon at incident electron energy $E = 2.222$ GeV and scattering angle $\theta = 15.54^\circ$. As observed in Fig. 3, the agreement between theory and data is very good over most of the energy spectrum, with some minor discrepancy seen only at the Δ -resonance peak. For completeness, we also present in this figure the electron-argon scattering spectrum measured at the beam energy $E = 700$ MeV and scattering angle $\theta = 32^\circ$ [59]. Note that the 2p-2h MEC response, peaked in the dip region between the QE and Δ peaks is essential to reproduce the data.

In the SLAC experiment [50] the inclusive cross sections $d\sigma/d\epsilon d\Omega$ for electron scattering on ^{12}C and ^{40}Ca were measured in the same kinematical conditions, i.e., at incident electron energy $E = 500$ MeV and $\theta = 32^\circ$. Using the SLAC and JLab data we estimated the measured $(Ca/C) = (d\sigma^{Ca}/d\epsilon d\Omega)_{nucl}/(d\sigma^C/d\epsilon d\Omega)_{nucl}$ and $(Ar/C) = (d\sigma^{Ar}/d\epsilon d\Omega)_{nucl}/(d\sigma^C/d\epsilon d\Omega)_{nucl}$ ratios, where the differential cross sections $(d\sigma^i/d\epsilon d\Omega)_{nucl}$ are scaled with the number of nucleons in the targets. Figure 4 shows the measured ratios as functions of energy transfer as compared to the RDWIA+MEC+RES calculations in the QE peak region. The calculated (Ca/C) [16] and (Ar/C) ratios agree with data where

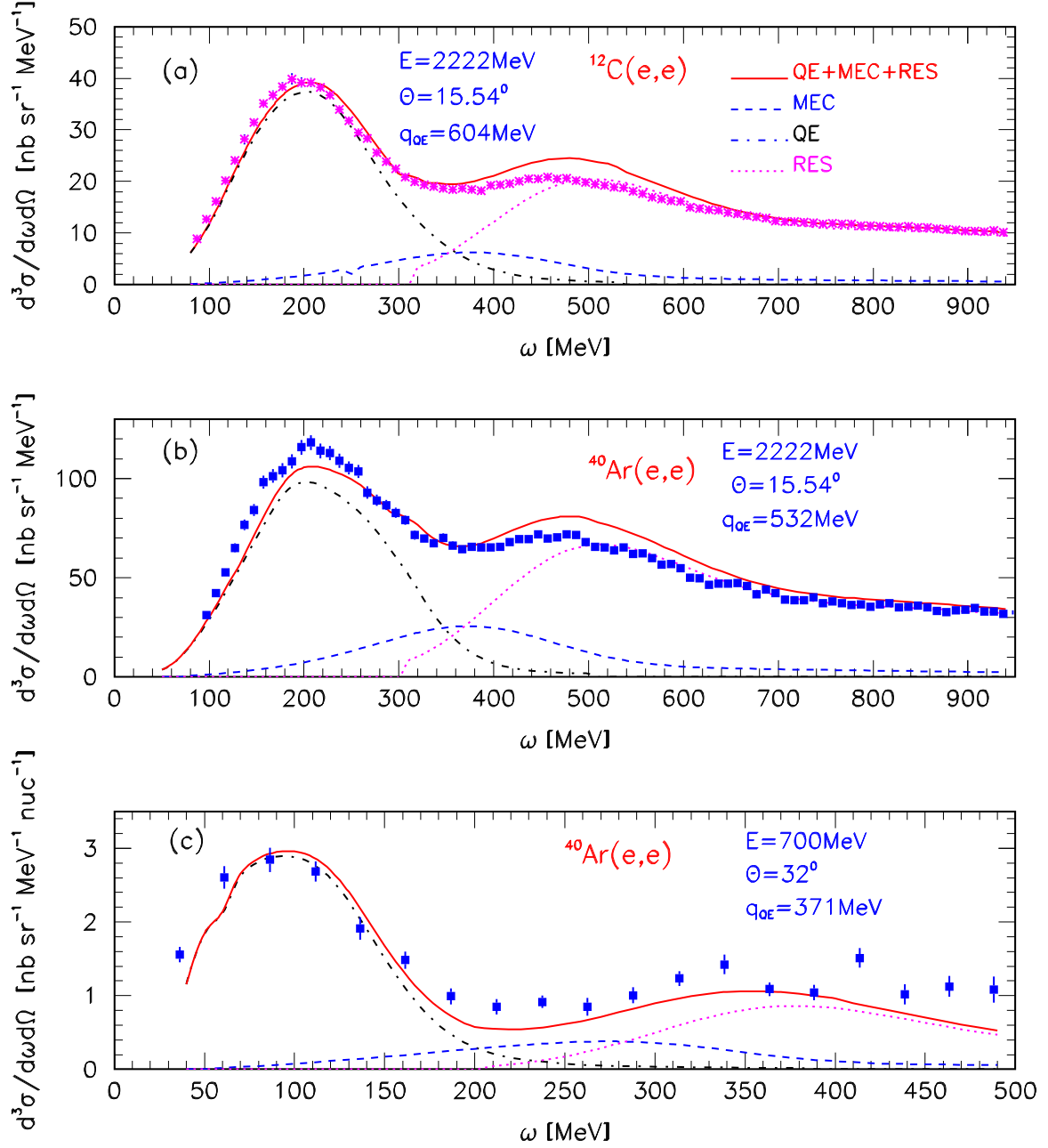


FIG. 3: The $^{12}\text{C}(e,e')$ (a) and $^{40}\text{Ar}(e,e')$ (b), (c) double differential cross sections of carbon and argon from Refs. [57, 58] vs energy transfer ω , compared with the RDWIA+MEC+RES prediction. The beam energy is $E = 2.222 \text{ GeV}$ and scattering angle $\theta = 15.541^\circ$. For completeness, data for electron scattering off argon at $E = 700 \text{ MeV}$ and $\theta = 32^\circ$ from Ref. [56] are also shown (c). As shown in the key, the separate QE, 2p-2h MEC, and inelastic contributions are presented.

the observed effects of $\approx 15\%$ in the QE peak region is higher than experimental errors. In Ref. [16] it was shown that the ground-state properties of these nuclei and FSI effects give the dominant contributions to the difference between the ^{12}C and ^{40}Ca (^{40}Ar) differential cross section per nucleon. The difference between the results for the carbon and argon targets is relevant in the context of Monte Carlo simulation for the DUNE neutrino oscillation experiment, where liquid argon and scintillator detectors are planned to be used as near detectors.

The agreement between theory and data in the dip region also gives us a confidence in the reliability of our calculations of the MEC effects. In this region the contributions emerge from the QE, 2p-2h MEC, and inelastic domains and can significantly overlap with each other making it difficult to experimentally separate the different reaction channels, for instance, the QE and two-nucleon knockout responses. Therefore, the comparison with data in this region can be considered to be a critical test for the validity of the RDWIA+MEC+RES approach, and particularly, the description of the 2p-2h MEC contribution that reaches its maximum value here. We can consider the difference between the calculated and measured cross sections observed at the maximum of the 2p-2h MEC contribution as a conservative estimate of the accuracy of the MEC response calculation in the vector sector of the electroweak interaction.

The electron scattering cross sections on carbon and calcium with scattering angle $\theta < 60^\circ$, corresponding to the kinematic of the neutrino oscillation experiments were analyzed. The $^{12}\text{C}(e, e')$ data were divided into two sets with electron energies $0.4 \leq E \leq 1.2$ GeV and $1.5 \leq E \leq 3.5$ GeV, that approximately corresponds to neutrino energies of the T2K (low energy) and NOvA (high energy) experiments.

We calculated $R_{dip}^i = (d\sigma^i/d\epsilon d\Omega)_{cal}/(d\sigma^i/d\epsilon d\Omega)_{data}$ ratios at the momentum transfer $|\mathbf{q}|_{dip}$ that corresponds to the minimum of the measured cross section, where $(d\sigma^i/d\epsilon d\Omega)_{cal}$ and $(d\sigma^i/d\epsilon d\Omega)_{data}$ are calculated and measured cross sections, correspondingly, for electron scattering off carbon ($i=\text{C}$) and calcium ($i=\text{Ca}$). The values of $|\mathbf{q}|_{dip}$ running from ≈ 250 MeV to ≈ 1100 MeV for carbon and $340 \leq |\mathbf{q}|_{dip} \leq 660$ MeV for calcium. We also calculated the 2p-2h MEC contributions to the (e, e') differential cross sections, i.e., $\delta_{MEC} = (d\sigma/d\epsilon d\Omega)_{MEC}/(d\sigma/d\epsilon d\Omega)$ ratios, where the $(d\sigma/d\epsilon d\Omega)_{MEC}$ is the 2p-2h MEC differential cross sections for electron scattering off nuclei. Figure 5 shows the ratios R_{dip}^i and δ_{MEC} as functions of $|\mathbf{q}|_{dip}$. The result presented in Fig. 5(a) demonstrates that the

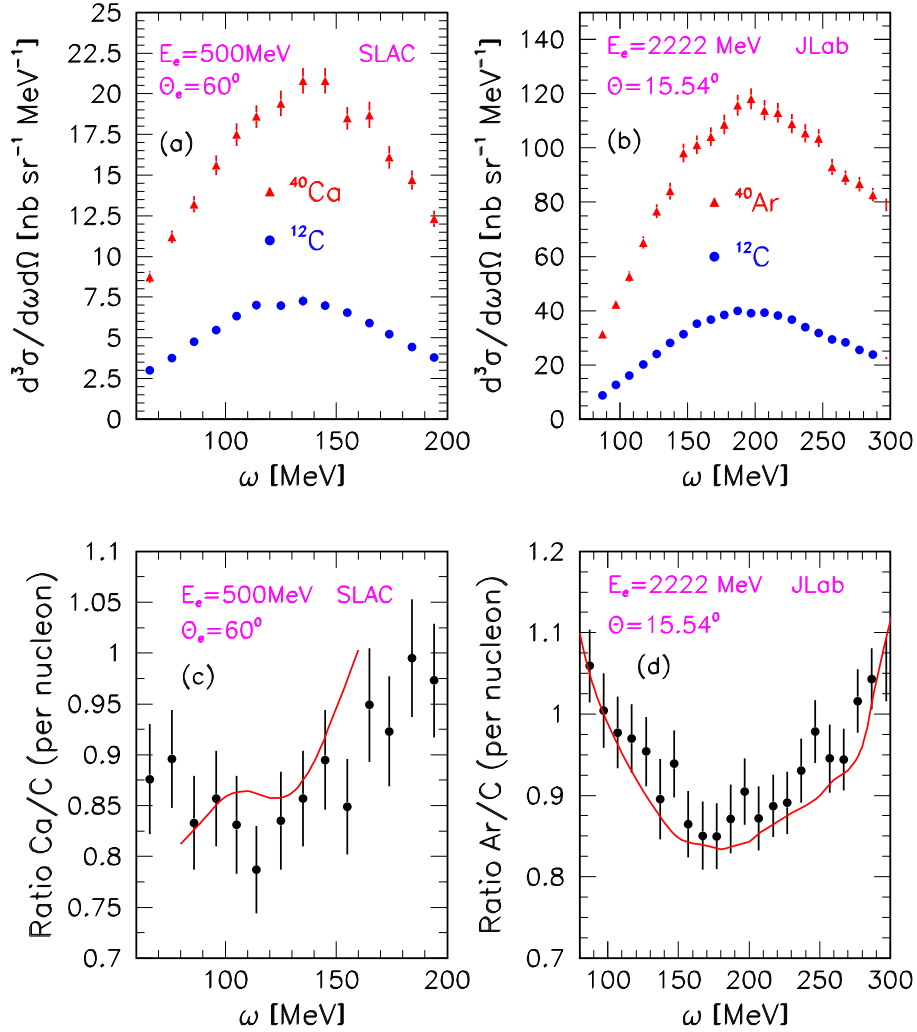


FIG. 4: The inclusive cross sections (a) and (b) and per nucleon cross section ratios Ca/C (c) and Ar/C (d) as functions of energy transfer ω for electron scattering on ^{12}C , ^{40}Ca , and ^{40}Ar . Data for ^{40}Ca and ^{12}C (a) are from Ref. [50] for electron beam energy $E = 500$ MeV and scattering angle $\theta = 60^\circ$. Data for ^{40}Ar and ^{12}C (b) are from Ref. [57, 58] for $E = 2222$ MeV and $\theta = 15.54^\circ$. The solid line is the result of the RDWIA+MEC+RES calculation.

R_{dip}^C ratio increases with $|\mathbf{q}|_{dip}$ from 0.7 at $|\mathbf{q}|_{dip} \approx 250$ MeV to ≈ 1 at $|\mathbf{q}|_{dip} \approx 500$ MeV and does not depend on electron energy. At $|\mathbf{q}|_{dip} > 500$ MeV the calculated and measured cross sections are in good agreement within the experimental errors. On the other hand the contribution δ_{MEC} [Fig. 5(c)] reduces with momentum transfer from 0.65 at $|\mathbf{q}|_{dip} \approx 250$ MeV to 0.42 at $|\mathbf{q}|_{dip} \approx 500$, and up to 0.2 at $|\mathbf{q}|_{dip} \approx 1000$ MeV and also does not depend on

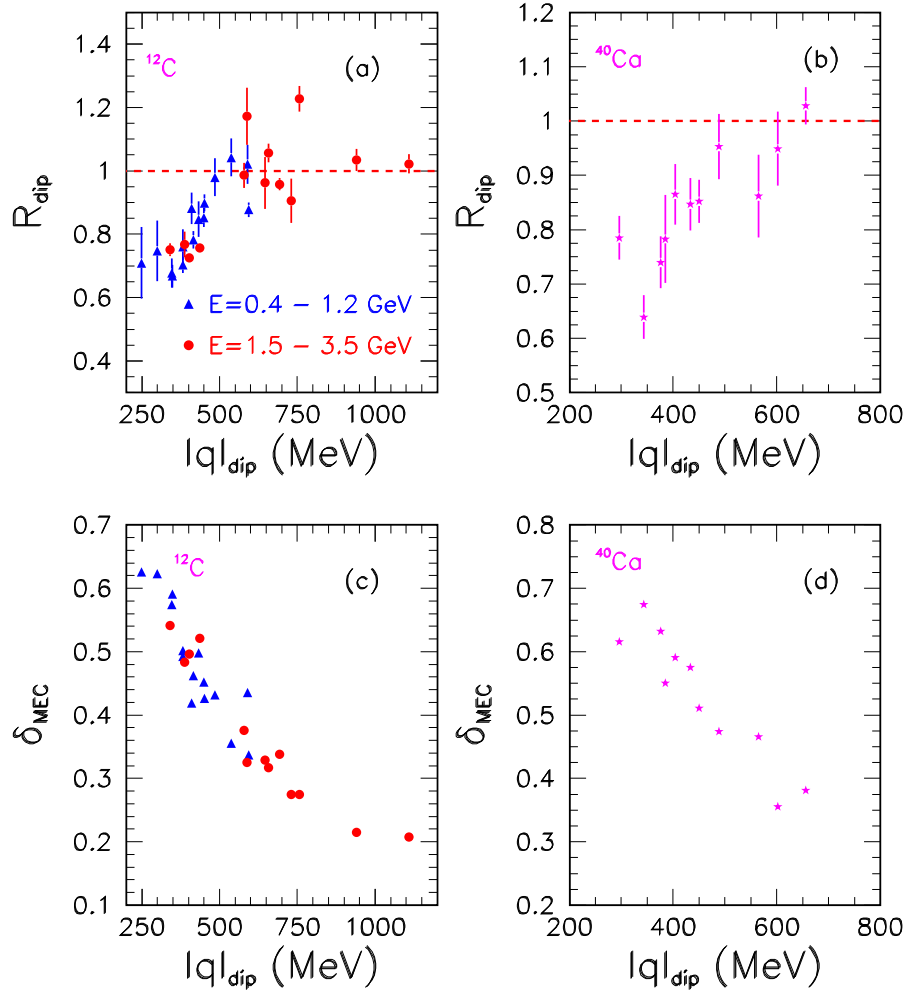


FIG. 5: Ratio R_{dip}^C for carbon (a) and R_{dip}^{Ca} for calcium (b) as a function of $|\mathbf{q}|_{dip}$. For carbon, data are from Refs. [54, 55] and for calcium from Ref. [56]. The ratios R_{dip}^C are shown for the two ranges of the incident electron energy $E = 0.4 - 1.2$ GeV (filled triangles) and $E = 1.5 - 3.5$ GeV (filled circles). The results of the RDWIA+MEC+RES calculation of the 2p-2h MEC contributions δ_{MEC} vs $|\mathbf{q}|_{dip}$ for electron scattering on carbon (c) and calcium (d). As shown in the key the contributions for carbon are shown for $E = 0.4 - 1.2$ GeV and $E = 1.5 - 3.5$ GeV.

the electron energy. The ratio R_{dip}^{Ca} [Fig. 5(b)] shows a similar dependence on $|\mathbf{q}|_{dip}$, i.e., R_{dip}^{Ca} increases with $|\mathbf{q}|_{dip}$ from 0.7 at $|\mathbf{q}|_{dip} = 350$ MeV to ≈ 1 at $|\mathbf{q}|_{dip} > 500$ MeV. The 2p-2h MEC contribution [Fig. 5(d)] decreases with momentum transfer from 0.68 at $|\mathbf{q}|_{dip} = 300$ MeV, and up to 0.38 at $|\mathbf{q}|_{dip} = 600$ MeV.

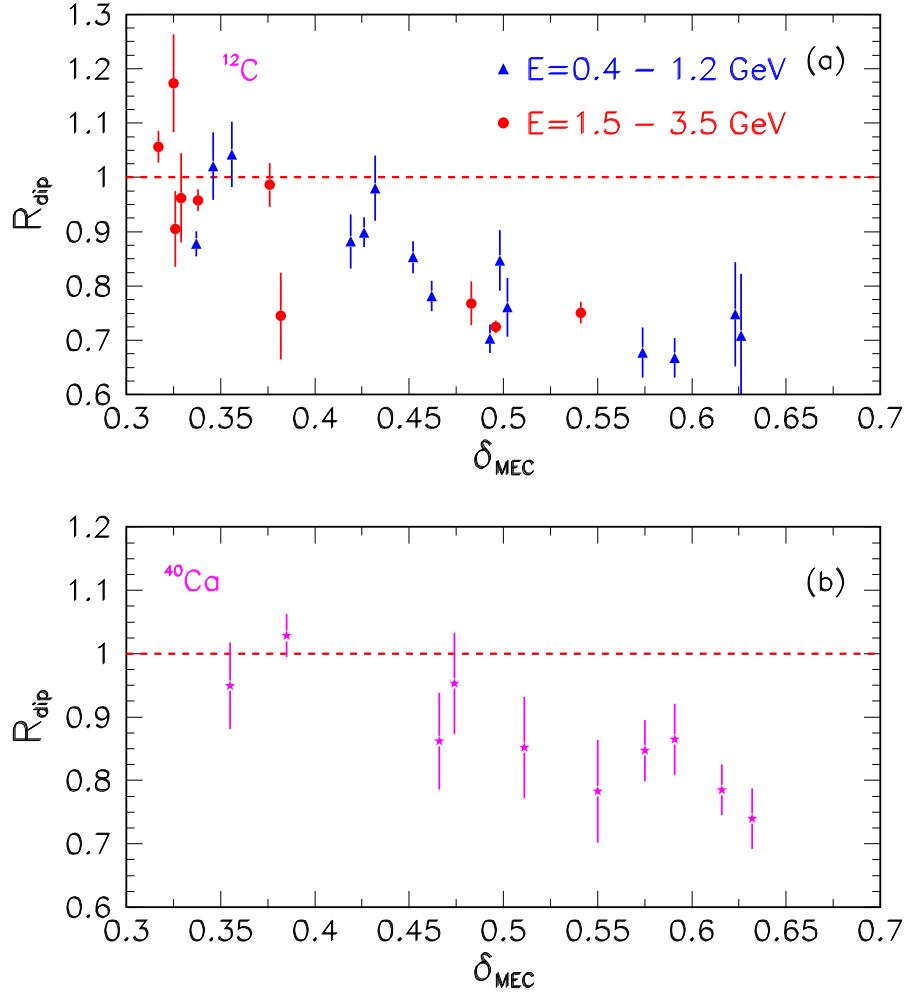


FIG. 6: Ratio R_{dip}^C for carbon (a) and R_{dip}^{Ca} for calcium (b) as a function of the 2p-2h MEC contribution δ_{MEC} , calculated in the RDWIA+MEC+RES approach. The ratios for carbon are shown for the incident electron energies $E = 0.4 - 1.2$ GeV (filled triangles) and $E = 1.5 - 3.5$ GeV (filled circles).

The R_{dip}^i ratios for carbon (upper panel) and calcium (lower panel) are shown in Fig. 6 as functions of δ_{MEC} . The figure shows that the $R_{dip}^i \approx 1$ up to $\delta_{MEC} \approx 0.45$ and then is reduced with δ_{MEC} to ≈ 0.8 at $\delta_{MEC} \approx 0.6$. Thus, the contribution of the 2p-2h MEC decreases with momentum transfer and the accuracy of the inclusive cross section calculated within the RDWIA+MEC+RES approach in the dip region improves with $|\mathbf{q}|_{dip}$ from 35% at $|\mathbf{q}|_{dip} \approx 250$ MeV ($|\mathbf{q}|_{dip} \approx k_F$) to 10% at $|\mathbf{q}|_{dip} \geq 500$ MeV ($|\mathbf{q}|_{dip} \geq 2k_F$), where k_F is

the Fermi momentum. We can use this estimation as conservative estimate of the accuracy of the 2p-2h MEC response calculation in the vector sector of the electroweak interaction.

IV. CONCLUSIONS

In this article, we studied the quasielastic, 2p-2h MEC, and inelastic electron scattering on carbon, calcium, and argon targets in the RDWIA+MEC+RES approach. This approach was extended to the whole energy spectrum, incorporating the contributions coming from the QE, inelastic and 2p-2h meson exchange currents. In calculation of the QE cross sections within the RDWIA, the effects of FSI and short-range NN -correlations in the target ground state were taking into account. An accurate parameterization of the exact MEC calculations of the nuclear response functions was used to evaluate the MEC response. The inelastic response functions were calculated using the parameterization for the neutron and proton structure functions. These functions were obtained from the fit of the measured inelastic electron-proton and electron-deuteron cross sections.

The present approach is capable of reproducing successfully the whole energy spectrum of (e, e') data at very different kinematics, including the recent JLab data for inclusive electron scattering on carbon and argon. It was shown that the measured and calculated in the RDWIA model the QE cross sections per nucleon target of electron scattering on ^{40}Ca (^{40}Ar) are lower than those for ^{12}C . The effect of 15% is observed in the QE region and is higher than experimental errors.

For electron scattering on the carbon and calcium targets we evaluated the ratios of the calculated inclusive cross sections to the measured ones at the momentum transfer $|\mathbf{q}|_{dip}$ that corresponds to the minimum of the measured cross sections in the dip region. We also estimated the 2p-2h MEC contribution to the (e, e') cross section at $|\mathbf{q}|_{dip}$. At the $|\mathbf{q}|_{dip} < 250$ MeV the RDWIA+MEC+RES approach underestimates the measured cross sections by about 30% and is in agreement with data within the experimental uncertainties at $|\mathbf{q}|_{dip} \geq 500$ MeV. The MEC contribution decreases with $|\mathbf{q}|_{dip}$ from 65% at $|\mathbf{q}|_{dip} = 250$ to 20% at $|\mathbf{q}|_{dip} = 1000$. These results depend weakly on electron beam energy. So, we validated the RDWIA+MEC+RES approach in the vector sector of the electroweak interaction by describing ^{12}C , ^{40}Ca , and ^{40}Ar data.

Acknowledgments

The authors greatly acknowledge J. Amaro and G. Megias for fruitful discussions and for putting in our disposal the codes for calculation of the MEC's electroweak response functions that were used in this work. We specially thank R. Kokoulin and A. Habig for fruitful discussions and a critical reading of the manuscript.

-
- [1] M. A. Acero *et al.*, (NOvA Collaboration), Phys. Rev. Lett. **123**, 151803 (2019).
 - [2] K. Abe *et al.*, (T2K Collaboration), Phys. Rev. Lett. **121**, 171802 (2018).
 - [3] R. Acciarri *et al.*, (DUNE Collaboration), FERMILAB-DESIGN-2016-03.
 - [4] K. Abe *et al.*, (Hyper-Kamiokande Collaboration) arXiv:1805.04163 [physics.ins-det].
 - [5] M. A. Acero *et al.*, (NOvA Collaboration), Phys. Rev. Lett. **D98**, 032012 (2018).
 - [6] T. Katori, M. Martini, J. Phys. **G45**, 013001 (2018).
 - [7] L. Alvarez-Ruso *et al.* Prog. Part. Nucl. Phys. **100**, 1 (2018).
 - [8] A. V. Butkevich and S. A. Kulagin, Phys. Rev. **C76**, 045502 (2007).
 - [9] A. V. Butkevich, Phys. Rev. **C80**, 014610 (2009).
 - [10] A. V. Butkevich, Phys. Rev. **C82**, 055501 (2010).
 - [11] P. G. Blunden and M. N. Butler, Phys. Lett. **B219**, 151 (1989)
 - [12] M. Martini, M. Ericson, and G. Chanfray, Phys. Rev. **C84**, 055502 (2011)
 - [13] M. Martini, and M. Ericson, Phys. Rev. **C87**, 065501 (2013).
 - [14] J. Nieves, I. Ruiz Simo, and M. J. Vicente Vacas, Phys. Lett. **B707**, 72 (2012).
 - [15] J. Nieves, I. Ruiz Simo, and M. J. Vicente Vacas, Phys. Lett. **B721**, 90 (2013).
 - [16] A. V. Butkevich, Phys. Rev. **C85**, 065501 (2012).
 - [17] M. Martini, N. Jachowicz, M. Ericson, V. Pandey, T. Van Cuyck, and N. Van Dessel, Phys. Rev. **C94**, 015501 (2016).
 - [18] I. Ruiz Simo, J. E. Amaro, M. B. Barbaro, A. De Pace, J. A. Caballero, and T. W. Donnelly, J. Phys. **G44**, 065105 (2017).
 - [19] G. D. Megias, T. W. Donnelly, O. Moreno, C. F. Williamson, J. A. Caballero, R. Gonzalez-Jimenez, A. De Pace, M. B. Barbaro, W. M. Alberico, M. Nardi, and J. E. Amaro, Phys. Rev. **D91**, 073004 (2015).

- [20] G. D. Megias, J. E. Amaro, M. B. Barbaro, J. A. Caballero, T. W. Donnelly, Phys. Rev. **D94**, 013012 (2016).
- [21] G. D. Megias, J. E. Amaro, M. B. Barbaro, J. A. Caballero, T. W. Donnelly, and I. R. Simo, Phys. Rev. **D94**, 093004 (2016).
- [22] Noemi Rocco, Carlo Barbieri, Omar Benhar, Arturo De Pace, and Alessandro Lovato, Phys. Rev. **C99**, 025502 (2019).
- [23] A. V. Butkevich and S. V. Luchuk, Phys. Rev. **C97**, 045502 (2018)
- [24] A. V. Butkevich and S. V. Luchuk, Phys. Rev. **D99**, 093001 (2019)
- [25] S. Dolan, G. D. Megias, and S. Bolognesi, Phys. Rev. **D101**, 033003 (2020).
- [26] M. B. Barbaro, J. A. Caballero, A. De Pace, T. W. Donnelly, R. Gonzalez-Jimenez, G. D. Megias, Phys. Rev. **C99**, 042501(R) (2019).
- [27] R. Gonzalez-Jimenez, A. Nikolakopoulos, N. Jachowicz, J. M. Udias, Phys. Rev. **C100**, 045501 (2019).
- [28] R. Gonzalez-Jimenez, M. B. Barbaro, J. A. Caballero, T. W. Donnelly, N. Jachowicz, G. D. Megias, K. Niewczas, A. Nikolakopoulos, J. M. Udias, Phys. Rev. **C101**, 015503 (2020).
- [29] A. Picklesimer, J. W. Van Orden, S. J. Wallace, Phys. Rev. **C32**, 1312 (1985).
- [30] J. M. Udias, P. Sarriguren, E. Moya de Guerra, E. Garrido, and J. A. Caballero, Phys. Rev. **C51**, 3246 (1995).
- [31] James J. Kelly, Phys. Rev. **C59**, 3256 (1999).
- [32] P. E. Bosted and M. E. Christy, Phys. Rev. **C77**, 065206 (2008).
- [33] M. E. Christy and P. E. Bosted, Phys. Rev. **C81**, 055213 (2010).
- [34] P. Mergell, U.-G. Meissner, and D. Drechsel, Nucl. Phys. **A596**, 367 (1996).
- [35] T. de Forest, Nucl. Phys. **A392**, 232 (1983).
- [36] B. Serot, J. Walecka, Adv. Nucl. Phys. **16**, 1 (1986).
- [37] C. J. Horowitz D. P. Murdock, and Brian D. Serot, in *Computational Nuclear Physics 1: Nuclear Structure* edited by K. Langanke, J. A. Maruhn, Steven E. Koonin (Springer-Verlag,Berlin, 1991), p.129.
- [38] D. Dutta *et al.*, Phys. Rev. **C68**, 064603 (2003).
- [39] J. J. Kelly, Phys. Rev. **C71**, 064610 (2005).
- [40] E. D. Cooper, S. Hama, B. C. Clark, and R. L. Mercer, Phys. Rev. **C47**, 297 (1993).
- [41] A. Meucci, C. Giusti, and F. D. Pacati, Nucl. Phys. **A739**, 277 (2004).

- [42] A. Meucci, C. Giusti, and F. D. Pacati, Nucl. Phys. **A765**, 126 (2006).
- [43] N. Rocco, L. Alvarez-Ruso, A. Lovato, and J. Nieves, Phys. Rev. **C96**, 015504 (2017).
- [44] C. Ciofi degli Atti and S. Simula, Phys. Rev. **C53**, 1689 (1996).
- [45] A. De Pace, M. Nardi, W. M. Alberico, T. W. Donnelly, and A. Molinari, Nucl. Phys. **A726**, 303 (2003).
- [46] E. Hernandez, J. Nieves, and M. Valverde, Phys. Rev. **D76**, 033005 (2007).
- [47] G. D. Megias, M. B. Barbaro, J. A. Caballero, J. E. Amaro, T. W. Donnelly, I. Ruiz Simo, J. W. Van Orden, J. Phys. **G46**, 015104 (2019)
- [48] G. D. Megias and J. E. Amaro, Private communication.
- [49] P. Barreau *et al.*, Nucl. Phys. **A402** 515, (1983).
- [50] R. R. Whitney, I. Sick, J. R. Ficenec, R. D. Kephart, and W. P. Trower, Phys. Rev. **C9**, 2230 (1974).
- [51] J. S. O'Connell, W. R. Dodge, J. W. Lightbody, Jr., X. K. Maruyama, J. O. Adler, K. Hansen, B. Schroder, A. M. Bernstein, K. I. Blomqvist, B. H. Cottman, J. J. Comuzzi, R. A. Miskimen, B. P. Quinn, J. H. Koch, N. Ohtsuka, Phys. Rev. **C35** 1063 (1987).
- [52] D. T. Baran, B. W. Filippone, D. Geesaman, M. Green, R. J. Holt, H. E. Jackson, J. Jourdan, R. D. McKeown, R. G. Milner, J. Morgenstern, D. H. Potterveld, R. E. Segel, P. Seidl, R. C. Walker, B. Zeidman, Phys. Rev. Lett. **61**, 400 (1988).
- [53] R. M. Sealock, K. L. Giovanetti, S. T. Thornton, Z. E. Meziani, O. A. Rondon-Aramayo, S. Auffret, J. P. Chen, D. G. Christian, D. B. Day, J. S. McCarthy, and R. C. Minehart, L. C. Dennis, K. W. Kemper, B. A. Mecking, J. Morgenstern, Phys. Rev. Lett. **62**, 1350, (1989).
- [54] O. Benhar, D. Day, and I. Sick, Rev. Mod. Phys. **80** 189 (2008).
- [55] O. Benhar, D. Day, I. Sick, Rev. Mod. Phys. arXiv:nucl-ex/0603032 (2006).
- [56] C. F. Williamson, T. C. Yates, W. M. Schmitt, M. Osborn, M. Deady, Peter D. Zimmerman, C. C. Blatchley, Kamal K. Seth, M. Sarmiento, B. Parker, Yanhe Jin, L. E. Wright, D. S. Onley, Phys. Rev. **C56**, 3152 (1997).
- [57] H. Dai *et al.*, Phys. Res. **C98** 014617 (2018).
- [58] H. Dai *et al.*, Phys. Res. **C99** 054608 (2019).
- [59] M. Anghinolfi *et al.*, J. Phys. G.:**21**, L9 (1995).